Towards an Understanding of the Fall Circumstances of the Hoba Meteorite

Martin Beech
Campion College, The University of Regina,
Regina, Saskatchewan, Canada S4S 0A2

Published in Earth, Moon and Planets: August 2013

Earth Moon Planets
DOI 10.1007/s11038-013-9421-7

Abstract

Using the observed attributes of the Hoba meteorite, that it is a single mass which survived impact intact, we investigate the possible conditions leading to its fall. Specifically, we asses the scenario in which the Hoba progenitor is envisioned as encountering Earth's atmosphere at a shallow angle of entry, with a low velocity and stabilized profile to the oncoming airflow. In order to physically survive impact we find, via the planar impact approximation, that the Hoba meteorite must have landed with a speed smaller than a few hundred meters per second. We find that the envisioned model can satisfy, in its extreme limit of low entry speed, maximum area profile and near horizontal entry angle the required landing conditions. We deduce that the progenitor mass for the Hoba meteorite was likely of order 5×10^5 kg, and that a simple impact crater, now eroded, having a diameter of some 20 meters and a depth of about 5 meters was produced upon impact. We estimate that the typical arrival time interval for such massive, Hoba-like meteorite falls is of order 5×10^6 years.

Key words: meteorites: Hoba; Earth impacts; planets and satellite: surfaces

1. Introduction

Records, as the old adage says, are meant to be broken. In terms of known meteorites the present record holder for the most massive find is that of the Hoba (Grootfontein) iron located in Namibia, Africa (Luyten, 1930; Fernie, 1967; Spargo, 2008). Discovered in 1920 (figure 1), and although a reflection of numerous selection effects (e.g., falling in a remote area, shallow surface burial, slow weathering and the fact that 71% of the Earth's surface is covered by oceans), the Hoba record has now held firm for more than 90 years. No greater single meteorite mass has been found nor has a more massive, non-fragmenting meteorite been observed to fall. While mass records have to begin and end somewhere, the Hoba meteorite is additionally notable with respect to the fact it is found in a landscape which shows no evidence of any significant impact alteration (figure 1).

With respect to its fall, we can say with confidence that the Hoba meteorite was either derived from a single, non-fragmenting parent body, or it is just the first found fragment, and not necessarily the largest fragment, in what is presumably a large and yet to be described strewn field produced by a disintegrated parent body. In addition, the absence of any accompanying impact features, in the modern era and indeed recorded history, implies that the meteorite was either transported from its original fall location, which seems highly unlikely, or that the fall circumstances were such that any initial impact signatures have now been eroded away. Both fall scenarios are interesting, and both have associated problem issues with explaining what is actually known about the meteorite.

Although a number of different scenarios are possible, some headway in understanding the Hoba fall can be made by testing a few of the more simple possibilities. In this sense we either find a straightforward model for the fall, which at least explains all the presently observed facts, or we can reject such models as being inadequate or over simplified and incapable of explaining the presently observed details. In this article we set out to determine the strengths, and any weaknesses, of the scenario which envisions the emplacement of the Hoba meteorite in a shallow impact structure (now eroded) as a single, non-fragmented mass that underwent a long, shallow-entry, low speed, orientation stabilized atmospheric flight.

2. Physical properties of the Hoba meteorite

Hoba is a nickel-rich, ataxite (IVB – Ni = 16.44 wt%) iron meteorite with an estimated mass of order 60,000 kg (Meteoritical Bulletin Database, 2011), and a formation age, based upon the rhenium to osmium radioactive decay chronometer of $4.3 \pm 0.3 \times 10^9$ yr (Hirata and Masuda, 1992) – an age not significantly different from that of the chondrite meteorites ($4.567 \pm 0.001 \times 10^9$ yr), and a result that is generally indicative of the parent planetesimals to iron meteorites undergoing a relatively rapid internal heating and differentiation phase once they formed. Hoba has a highly homogeneous structure, even on scales as small as a few tenths of a millimeter, and it has been used as a concentration standard in metallurgic trace element studies (Cook et al, 2006). The cosmic-ray exposure (CRE) data, derived from the measured ^{3}He and ^{4}He abundances, indicates that the fragmentation event resulting in the production of Hoba's parent meteoroid occurred some 200 million years ago (Bauer, 1963). Indeed, making use of this relatively long CRE age, Jones et al (1989) used several microgram fragments of the Hoba meteorite to search, unsuccessfully as it turned out, for fractionally charged particles that might have (theoretically) been accreted by the meteorite while exposed to space.

Hoba's approximate shape is that of a square slab with dimensions of 2.95 x 2.84 x 0.9 meters (Spencer, 1932); it shows no significant cracks or obvious fracture planes (McCorkell et al, 1968). The meteorite has suffered some considerable surface contact alteration, having developed a thick 20 to 30-cm iron-shale base where it contacts the underlying Kalahari limestone (Spencer, 1932; Golden, Ming and Zolensky, 1995). Based upon ^{59}Ni radionuclide studies McCorkell et al (1968) deduce a terrestrial residency time of less than 80,000 years. This relatively long, by human standards, residency time clearly dictates that, sadly, no written or even ethno-historic record of its actual fall will ever be found.

The condition for atmospheric fragmentation is typically set according to the ram pressure P_{ram} exceeding the yield strength of the meteoroid material Y. In this manner once $P_{ram} = \rho_{atm} V^2 > Y$, where ρ_{atm} is the atmospheric density and V is the velocity of the

meteoroid, so the meteoroid will begin to fragment. This condition, however, is usually modified according to the Weibull statistical strength theory to account for the effects of internal fracture plains and structural defects. Accordingly, the strength of the meteoroid material is written as $Y = Y_0(m_0 / m)^{\alpha}$, where Y_0 and m_0 are reference values derived from laboratory testing, m is the instantaneous meteoroid mass and α is a constant typically of order 0.25 for meteorites (Svetsov, Nemchinov and Teterev, 1995). Such modeling was applied by Pierazzo and Artemieva (2005), for example, in their study of the possible atmospheric fragmentation modes of the iron asteroid responsible for the production of the Canyon Diablo crater and its associated meteorite (iron IAB-MG, Ni = 7.17%) strewn field. There are currently no published test data concerning the appropriate Y_0 and m_0 values for the Hoba meteorite, but Furnish et al (1995 – their figure 5) report an experimentally measured yield strength value of some 700 MPa for a small fragment of the Hoba meteorite. Svetsov, Nemchinov and Teterev (1995) indicate that the tensile strength for the Sikhote-Alin (IIAB – Ni = 5.8 wt%) iron meteorite is 44 MPa, while the compressive strength for the Charcas (a.k.a. Descubidora, IIIAB - Ni = 7.86 wt%) iron is 380 MPa. From this, we determine, that the yield strength of ataxites, and specifically that of Hoba, is appreciably higher than that derived for medium-octahedrite and hexahedrite iron meteorites - e.g., Petrovic (2001) finds that the average compressive strength of such meteorites is 430 MPa, with the average tensile strength being 45 MPa. Based upon the measured data point presented by Furnish et al (1995), the yield strength of the Hoba meteorite would appear to be very high, and at face value this supports the possibility that it is derived from a non-fragmented, mono-ferric mass. The high degree of structural homogeneity exhibited by the Hoba meteorite (Furnish et al, 1995; Cook et al, 2006) further suggests only a small mass (that is size) dependency upon Hoba's compressive properties – in which case the Weibull parameter α will likely be small and close to zero in value and the m_0 term will be largely irrelevant. For all of the above comments and qualifications, however, the computer simulations (to be described below) track the variations in the ram pressure that a Hoba-like meteoroid will experience as it moves through the atmosphere and the ram pressures encountered in these simulations never exceed 100 MPa, and indeed, are typically half to one-quarter of this value. In addition to the above qualifications, it is also worth drawing attention to the fact even

large stony meteorites, which have much lower compressive strengths than irons (Popova et al., 2011) can survive atmospheric passage without fragmenting (Borovicka and Spurny, 2008). The best, most recent example of this is the Carancas meteorite fall of 15 September, 2007 in Peru. In this particular case an estimated 5000 kg initial mass, 2-m diameter, H4 chondrite meteoroid (Tancedi et al, 2008; Brown et al, 2008) penetrated Earth's atmosphere with an initial velocity of some 15 km/s but did not fragment until it hit the ground – at which instant a 13-m wide crater was produced.

The deformation characteristics of a metal vary according to temperature, and to this end Johnson, Remo and Davis (1979) have studied the low temperature impact characteristics of a Hoba meteorite fragment. They find that a brittle to ductile fracture transition will occur at a temperature of order 150 K; a result which suggests that during impact formation from its parent asteroid, and during its atmospheric interaction, the Hoba iron would have ductile rather than brittle characteristics – for the progenitor production event we assume a 2.7au orbital radius to an M-type asteroid having an albedo of $A = 0.15$, and derive an equilibrium temperature of ~165K. At Earth orbit the equilibrium temperature is ~ 280K. All in all, the available published data on the Hoba meteorite indicate a highly coherent, ductile body with a yield strength containing few structural defects.

That the Earth impact speed, V_{imp}, of the Hoba iron must have been substantially less than its pre-atmosphere encounter velocity, V_{∞}, is evidenced by the lack of any long-lived and significant structural deformation of its standing limestone substrate. While the impact velocity threshold beyond which crater formation must inevitably take place is not well known, clearly, the smaller the impact speed the better, since then the associated kinetic energy of impact will itself be small. In general, impact velocities greater than about 12 km/s are considered to be high enough to completely melt and vaporize any impacting meteoroid - irrespective of its composition (Okeefe and Ahrens, 1982; Melosh, 1989). With respect to possible impact speeds for the Hoba meteorite, Buchwald (1975, his figure 864) interestingly finds that a large (135 cm^2) polished surface section shows an orientated sheen that is indicative of some slight shock deformation (figure 2). Laboratory experiments carried out by Bland et al (2001) upon Gibeon (IVA – Ni =

7.7%) iron meteorite fragments find that structural deformation occurred once the impact velocity was greater than ~1 km/s. On this basis we would suggest that the available physical evidence supports the idea that the Hoba meteorite landed relatively softly, with a low impact speed. This being said, perhaps the more useful question to ask is, "what is the maximum possible impact velocity that the available data will support?"

The apparent fact that the Hoba meteorite survived impact *en masse* imposes perhaps the strongest constraint upon the range of possible impact speeds. Indeed, by using the planar impact approximation and the relatively well known physical properties of the Hoba meteorite and its target material an upper limit on the impact speed allowing survival can be obtained. Accordingly, the standard Hugoniot shock equations (see e.g., Melosh. 1989) have been used to model the variation in the properties of interest. For the target material we adopt equation of state parameters provided by Ahrens, Anderson and Zhao (1995) for limestone with impact velocities smaller than 2 km/s. For the Hoba meteorite, we adopt the iron equation of state parameters given by Melosh (1989). Our calculations indicate that for an impact velocity of 1 km/s a shock pressure of 7.6 GPa is induced in the projectile and under these circumstances the Hoba meteorite would definitely not survive. At 0.5 km/s impact velocity, the shock pressure in the projectile is more than halved to some 3.1 GPa, but this is still well above the survival limit for the Hoba Meteorite. Only at impact velocities smaller than ~ 0.25 km/s do we find shock pressures below 1 GPa. Taking, therefore, an absolute upper limit of 700 MPa (Furnish et al, 1995) as a survivable value against shock disruption, we estimate that the impact velocity for the Hoba meteorite must have been smaller than a few hundred meters per second. At this impact speed the shock induced within the target area will still exceed the yield strength of limestone by about one order of magnitude, and accordingly some impact related structure must have been produced at the time of the meteorite's fall.

Crater formation, as is well known, is not only dependent upon the impact velocity; it also varies in a complex manner with the target material density and the impact angle (for a general review see e.g., Melosh, 1989). Davison et al (2011) along with Collins et al (2011) have recently reviewed the effects of varying impact angle upon crater size and

crater morphology, and note that both small-scale laboratory experiments and numerical modeling indicate that as the impact angle decreases (that is become closer to glancing) so the impact crater depth decreases, and the along-range crater profile becomes increasingly asymmetric. Additionally, once the impact angles decreases below a material dependent threshold value so the crater planforms become more and more elliptical with larger and larger amounts of decapitated impactor material being deposited downrange. Bottke et al (2000) argue that the ellipticity threshold horizon angle for planetary targets (based upon studies of Martian, Cytherean and Lunar craters) is about 12^o. Impact experiments carried out in the laboratory further indicate that the critical angle can be as small as 5^o for a sand target, but as large as 30^o for a granite target (Davison et al, 2011 – see their table 1). Although a shallow elliptical impact crater on Earth's surface would be difficult to recognize (being subject to relatively rapid erosion and weathering) the laboratory and numerical simulations indicate that impact velocities in excess of several kilometers per second are still required for the actual excavation process to proceed. No detailed survey for shock metamorphic materials (shatter cones) or crater lens related breccia in the area immediately surrounding the Hoba meteorite has ever been published (see, however, the general area description given by Fernie 1967), and even so, the likelihood of finding any traces of a shallow elliptical crater surviving after a time equivalent to the Hoba residency age seems unlikely. It is perhaps worth pointing out at this stage that the greater region around the fall site has been extensively surveyed with respect to its potential for commercial mining, and the Grootfontein region supports a number of copper, zinc, cadmium and vanadium mining enterprises. One would suspect, therefore, that if Hoba is part of an extensive strewn field then some evidence of its existence (through the discovery of the more numerous smaller masses) would have, by now, been made. Unfortunately, therefore, there appear to be no obvious geographical, land-survey, or crater morphology constraints on the exact landing circumstances and/or impact angle of the Hoba meteorite.

Based upon the discussion presented above we shall assume in the analysis below that the Hoba meteorite impacted Earth's surface with a characteristic velocity of no more than a few hundred meters per second with $V_{\rm imp} < 0.25$ km/s. The maximum kinetic energy of

impact due to the Hoba meteorite would therefore be of order $E_{imp} \sim 10^9$ J (about 290 kg of TNT equivalent energy). Energies of this order of magnitude will cause only local damage and deformation at the impact site (see Section 6 below).

3. Earth encounter

The typical Earth encounter velocity (V_∞) of potential Earth impacting iron meteorites is given by Bottke et al (1994) as between 12 and 20 km/s – the absolute minimum meteoroid encounter speed is that of Earth's escape velocity: 11.2 km/s. Survival against impact destruction is entirely dependent, therefore, upon the amount of atmospheric deceleration that a meteoroid experiences. Melosh (1989) indicates that, as a rule of thumb, a meteoroid will be significantly decelerated if it encounters more than its own mass in the atmospheric column traversed. The atmospheric column mass per unit area can be deduced from the equation of hydrostatic equilibrium: $dP / dl = - g \rho_{atm}$, where P is the atmospheric pressure and g is the surface gravity. For a constant entry angle θ, where $\theta = 90^o$ corresponds to a vertical trajectory, the atmospheric column mass per unit area M_{col} is $M_{col} = \int_0^\infty \rho_{atm}\, dl$, where it is assumed in the integral that the entire Earth atmosphere has been traversed. Accordingly, $M_{col} = P_0 / [g \cos(\theta)]$, where P_0 = 101,325 Pa is the atmospheric pressure at sea-level. If an impacting meteoroid has a surface area of atmospheric interaction A and volume U, then the condition for substantial deceleration is that the meteoroid mass $M_{met} = \rho_{met}\, U \leq M_{col}\, A$, where ρ_{met} is the density of the meteoroid material. This relationship sets a constraint on the meteoroids volume-to-mass ratio of $U/A < M_{col} / \rho_{met} = P_0 /[\rho_{met}\, g \cos(\theta)]$ - meters. Substituting appropriate values for P_0, g = 9.81 m/s^2, and ρ_{met} = 7800 kg/m^3 (the density of nickel-iron meteorites), we find $U/A < 1.32 \sec(\theta)$ - meters.

The volume-to-area ratio for a sphere of radius R is simply $R / 3$. For a square faced prism of side L and depth D, appropriate to the form of the Hoba meteorite, the volume will be L^2D, but the cross-section area of interaction with the atmosphere can vary between the two extremes of L^2 (square face-on) to LD (rectangular edge-on). Accordingly we have $D < U/A < L$. While at this stage (but see below) the pre-

atmosphere interaction size of the Hoba meteorite is not known, assuming that its atmospheric flight was stable (again see below) and that the same profile was directed towards the direction of motion, then we can take bounds of order $1.5 < U/A < 3.5$. Accordingly the maximum values for the horizon angle are $\theta < 28^o$ (for $U/A = 1.5$) and $\theta < 68^o$ (for $U/A = 3.5$). These results suggest quite a large range of entry angles might be available to the Hoba meteorite progenitor – but such a conclusion, being based upon a rule of guiding thumb argument, clearly requires a more detailed evaluation (see below).

Shoemaker (1962) has shown that for an isotropic flux the probability dP that the angle of impact θ will fall in the range Ψ to $\Psi + d\Psi$ is independent of the gravity of the target body, and that $dP(\Psi < \theta < \Psi + d\Psi) = \sin(2\Psi)\, d\Psi$, indicating that the most likely impact angle of impact is 45^o. Pierazzo and Melosh (2000) further note that of order 77% of meteoroid encounters will have impact angles in the range $20 < \theta^o < 70$, with less than 1% of encounters having impact angles smaller than 5^o. Additionally, however, we note that 50% of all meteoroids enter the Earth's atmosphere at angles of 30^o or less to the horizon (Melosh – personal communication). Accordingly, the Hoba meteorite only begins to enter the more rare class of Earth encountering objects if its trajectory angle is found to be much smaller than some 10 to 15^o.

While rapid spin effects are taken to be negligible with respect to the ablation process in this analysis, some rotation (but not random tumbling) is none-the-less envisioned in order to stabilize the flight orientation. Accordingly we adopt the approach that the ablation profile of the meteoroid remains constant as it moves along its atmospheric path. The analogy being adopted here is with the stabilized flight responsible for the production of shield and orientated meteorites, many examples of which are known to exist within museum collections from around the world. Under this approximation we are knowingly biasing our study towards testing the most favorable atmospheric deceleration conditions – the idea being that if the Hoba mass cannot be slowed sufficiently with its maximal possible area of interaction, then it certainly cannot be slowed sufficiently, *mutatis mutantis,* with a smaller area.

4. Atmospheric flight model

To recap: the model being tested here is that in which the Hoba meteorite fall is the end result of a non-fragmenting meteoroid entering into Earth's atmosphere with a stabilized profile along a shallow entry angle path at the slowest possible entry speed of 11.2 km/s. The equations of motion and mass loss ablation that have been followed numerically are described in the Appendix [see also Beech (2011) where the code was used to investigate the characteristics of Leonid meteors]. Our procedure adopts a two dimensional, curved-atmosphere geometry allowing for over the horizon, long flight-time simulations to be made. In assuming an orientated flight, the meteoroid provides a constant surface area S of interaction to the on-coming air flow. Accordingly the two extremes that are allowed for are $S = L^2$ (square face-on), and $S = LD$ (edge-on). The models are further characterized by adopting a range of values of the ablation coefficient $\sigma = \Lambda / 2\ \Gamma\ \zeta$, where Λ is the heat transfer coefficient, Γ is the drag coefficient and $\zeta = 5 \times 10^6$ J kg^{-2} is the enthalpy of melting and vaporization appropriate for iron meteorites (Passey and Melosh, 1980). A constant drag coefficient of $\Gamma = 1.2$ has been adopted for the calculations in this study, this being taken as a representative value based upon the typical drag coefficients (see e.g., figure 9.19 and 9.20 of Young et al, 2010) derived for a cube ($\Gamma = 1.05$), a rectangular prism ($\Gamma = 2.1$), a square flat plate ($\Gamma = 1.17$), a long cylinder ($\Gamma = 0.82$), and a short cylinder ($\Gamma = 1.15$). We acknowledge that the value of the drag coefficient will vary according to atmospheric height, being as it is a complicated function of the Reynolds number of the on-coming airflow and the reactive momentum of the reflected and evaporating molecules (Bronsheten, 1983; Melosh and Goldin, 2008) - the consequences of varying this term are evaluated in section 5 below. The heat transfer coefficient is one of the least well known terms in all of meteor physics, but it is typically taken to reside in the range $0.005 < \Lambda < 0.5$ (Bronshten, 1983 – his figure 16; Svetsov, Nemtchinov and Teterev, 1995 – their table 1). With the range of parameters described the ablation coefficient adopted in the numerical simulations is taken to have extreme values of $5 \times 10^{-10} < \sigma\ (\mathrm{s^2 m^{-2}}) < 5 \times 10^{-8}$. This range for the ablation coefficient covers those adopted by other authors in similar such studies as this one (Baldwin and Sheaffer, 1971; Passey and Melosh, 1980; Pierazzo and Artemieva, 2005). The upper value end of our range also includes that specified for iron meteorites

by ReVelle and Ceplecha (1994). These authors advocate a high effective value of σ (s^2m^{-2}) ~ $4x10^{-8}$ based upon observational as well as (unpublished) laboratory data (ReVelle and Ranjan, 1988). An additional factor that we do not attempt to address in this study is that in which the various terms entering into the evaluation of the ablation coefficient change according to meteoroid shape, velocity and mode of ablation (that is mass loss via surface vaporization, surface melting and/or quasi-continuous detachment of small fragments – Bronshten, 1983, his table 31; Ceplecha and ReVelle, 2005).

In addition to the drag coefficient, the equations describing the meteoroids flight (see the Appendix) also include a lift coefficient term (see equation A3). In general this term is taken to be small $C_{lift} \approx 0$, and is accordingly ignored, but since we allow for potentially long atmospheric paths at a shallow angle to the horizon it can in principle take-on values in the range $-0.5 < C_{lift} < 1.0$ dependent upon the angle of attack; for face-on angles of attack, however, $C_{lift} \equiv 0$ (Matsumoto et al, 1998 – their figure 7) and this is the adopted value in this study.

All of the simulations adopt a starting altitude of 500 km (see the Appendix for a discussion on this point), with the initial velocity being chosen in the range $11.2 < V_\infty$ (kms^{-1}) < 20, and the initial impact angle varying between 0 (horizontal) < θ^o < 90 (vertical). No ablation takes place in the attitude range between 500 and 100 km, but the high starting point does allow for the possible gravitational alteration of the meteoroids flight path – the ground path parameter is somewhat arbitrary, therefore, and simply keeps track of the computed range rather than describing the luminous (or active ablation) ground path. The initial mass is taken to be $m = \rho_{met} A D_0$, where D_0 is the initial meteoroid depth length. The area of atmospheric interaction is allowed to vary between the two extremes of $A(m^2)$ = 2.95 x 2.84 (large face forward) and $A(m^2)$ = 2.84 x 0.9 (small face forward). Although we model and account for the ablation mass loss in this face-on manner, emphasizing thereby the specific affects of the meteoroid's area of interaction with the on-coming air flow, we certainly expect the entire meteoroid surface to show signs of ablative mass loss – as indeed, the regmaglypts on the surface of the Hoba meteorite indicate (figure 1). This latter phenomenon, of course, relates to the effect

of the hot, turbulent gas flow moving around the entire meteoroid body. The input parameters for the numerical models are summarized in table 1.

Table 1 in here

5. Numerical simulations

Before considering the detailed, Hoba-specific, fall conditions we first look at a few general simulations to test the veracity of our numerical code. Table 2 presents the results from a series of simulations for a 10^5 kg initial mass meteoroid. Various entry velocities, ablation coefficient, entry angle and surface areas are compared.

Table 2 in here

Reassuringly, from table 2, we find that the atmospheric flight path characteristics are consistent with initial (broad-brush form) expectations. Firstly, the ground path is shorter when the larger face is orientated towards the oncoming air flow (column 5 of table 2) – this is a consequence of the greater atmospheric deceleration experienced when orientated in this fashion. Indeed, *ceteris paribus*, when the smaller face orientation condition holds the impact speeds are larger, by a factor between 3 and 10, when compared to those with the larger face orientated forward. Second, the smaller the ablation coefficient, so the smaller is the initial progenitor mass needed to produce a specific mass meteorite upon the ground (column 6 of table 2). Third, the smaller the atmospheric entry angle (for a fixed speed and initial mass) so the longer is the atmospheric flight path, the smaller is the ground impacting mass and the smaller is the impact velocity (see columns 5, 6, and 8 of table 2). In addition, when the initial velocity is 11.2 km/s, we find from our simulations that the initial entry angle (at 500 km altitude – see the Appendix discussion) must be greater than 16^o if the meteoroid is to physically impact upon Earth's surface. Smaller entry angles than this result in the meteoroid suffering a fate similar to that observed for the 10 August 1972 fireball which traversed an approximate 1500 km ground path over western North America and Canada (Rawcliffe et al, 1974; Ceplecha, 1994) before returning back into interplanetary space.

As the atmospheric entrance speed increases, so the entry angle for Earth impact also increases: at 20 km/s the Earth impact condition requires horizon entry angles of $\theta > 20^{o}$ (at 500 km altitude). The non-fragmentation condition is tested in our numerical simulations by following the ram pressure experienced by the meteoroid, and, as expected for a given initial mass, profile and speed the maximum ram pressure experienced increases with increasing entrance angle. The closer the angle of entry is to the vertical so the shorter is the meteoroid's flight path, the smaller is its total deceleration and the higher is the maximum ram pressure experienced (column 9 of table 2). With an entrance velocity of 11.2 km/s, we find that for a 10^5 kg progenitor, with its large face forward and σ (s^2m^{-2}) = 1.0 x 10^{-8}, the maximum ram pressure experienced is 39 MPa, at a height of 10.0 km, for a vertical flight path; when $\theta = 16^{o}$, the maximum ram pressure experienced is reduced to 2.2 MPa, at a height of 23.5 km altitude. Similar such results, although with higher maximum values (by a factor of about 3) for the ram pressure are obtained when the smaller face is orientated forward – this is a again a result of the smaller deceleration experienced by a meteoroid orientated in this manner. The effect of changing the drag coefficient adopted in the simulations can be gauged from table 2 in the sense that, all other terms being held constant, a decrease in the drag coefficient (smaller than our adopted $\Gamma = 1.2$ that is) will result in an effective increase in the ablation coefficient. Consequently, we see that the smaller the value for the adopted drag coefficient so the lower is the impact velocity (table 2, column 6). Additionally, an increased ablation coefficient (that is, a reduced drag coefficient *ceteris paribus*) results in a greater amount of meteoroid mass loss during atmospheric flight, and accordingly the larger must the initial meteoroid mass be in order to produce an appropriate Hoba mass meteorite on the ground. Table 2 column 9 further indicates that, all else being the same, the enhanced mass loss and speed reduction resulting from a smaller drag coefficient culminate in a meteoroid experiencing a smaller maximum ram pressure – a result that favors non-fragmentation. The converse of the above discussion points will apply if the drag coefficient is increased above our adopted value of $\Gamma = 1.2$, but even with the smallest likely value for the heat transfer coefficient ($\Lambda \sim 0.01$) so a constant drag coefficient as high as 2.0 (resulting in σ (s^2m^{-2}) ~ 5 x10^{-10}) can still produce, albeit only just, a Hoba mass meteorite on the ground. In general, therefore, we find that for slow

initial speeds and shallow entrance angles the maximum ram pressure experienced by a potential Hoba meteorite precursor is one to two orders of magnitude smaller than the maximum yield strength determined for ataxite material (Furnish et al, 1995). Under these circumstances, it would appear that the non-atmospheric fragmentation assumption for the Hoba precursor meteoroid is a sound one.

In the remainder of this analysis we shall investigate the most favorable circumstances under which a Hoba mass meteorite might have been produced. Accordingly, we set the entrance speed to be 11.2 km/s (the slowest possible), the entrance angle to be 16^{o} (the smallest angle, at 500 km altitude, for producing a ground impact – this is also the longest atmospheric path model), and we take the largest face to be orientated forward (this maximizes the area exposed by the meteoroid to the on coming airflow, and it also maximizes the deceleration). With these conditions fixed, the remaining variable is the initial mass and then the various quantities that determine the ablation coefficient. Figure 3 shows the obtained variations in the impact speed for a range of initial masses and adopted ablation coefficients. Again, the results presented in figure 3 follow expectation – for a given initial mass, the larger the ablation coefficient so the greater the mass lost during atmospheric flight, the smaller the impacting ground mass, and the lower the impacting speed. What we now seek to find are the conditions under which a Hoba mass meteorite might be deposited upon the ground (for a given initial mass and ablation coefficient). The vertical line in the center of figure 3 indicates the boundary at which the impacting ground mass is 60,000 kg (i.e. the mass of the Hoba meteorite. We find from our simulations that under the most ideal of circumstances, it is certainly possible to produce a Hoba mass impactor with a speed smaller than a few hundred meters per second (technically the minimum found is 220 m/s) - impacting speeds smaller than 100 m/s are possible, but only for a ground masses smaller than that of the Hoba meteorite. From figure 3 we see that, for example, that when $\sigma (s^2m^{-2}) = 1.0 \times 10^{-8}$ a Hoba mass meteorite will impact the ground at a speed of about 200 m/s when the initial mass is 1.15×10^5 kg. For $\sigma (s^2m^{-2}) = 2.5 \times 10^{-8}$, a Hoba mass meteorite is produced by a meteoroid having an initial mass of 3.1×10^5 kg. According to the parameter set leading to figure 3, increasing either or both the initial encounter speed and entrance angle, for a

given initial mass and ablation coefficient, smaller ground masses impacting at higher speeds will be obtained. There is some small amount of wiggle-room (due to the range of uncertainty in the ablation coefficient) with respect to producing a Hoba mass meteorite on the ground from slightly higher initial velocity and slightly higher initial entrance angle progenitors.

At face value our numerical simulations indicate that under the most favorable of atmosphere encounter conditions it is possible to produce a Hoba mass meteorite upon the ground with an impact velocity of order a few hundred meters per second. Smaller impact speeds than 200 m/s might well be realized by additional adjustment of the model input parameters, but this soon begins to over-state the exactness of the input physics – that is, the limitations of the planar impact approximation and the physics of the ablation process. It seems reasonable to conclude, however, that the non-fragmenting, low velocity, low entry angle, stabilized flight model can explain the fall circumstances of the Hoba meteorite, all-be-it at close to the limit of its applicability. Accordingly it would appear that for ablation coefficients in the range $5 \times 10^{-9} < \sigma (s^2 m^{-2}) < 5 \times 10^{-8}$ an intact Hoba mass (ataxite) meteorite can be produced by progenitor objects with initial masses in the range $10^5 < M_\infty (kg) < 10^6$ respectively (see figure 3).

6. Discussion

The fact that the non-fragmenting, low velocity, low entrance angle, stabilized flight model can account for the fall circumstances of the Hoba meteorite does not allow us to exclude the more dynamic, fragmenting progenitor scenario. This being said, if one wishes to invoke the latter model, then the question of the (apparently) missing siblings and associated strewn field arises. Importantly, however, it should be possible to distinguish between the two models through the initiation of extensive fieldwork - although the terrain, climate and location are not ideal for such survey work. Grootfontein is located in an ostensibly agricultural area, with much of the surrounding land surface being used for arable crops (mostly maize) and cattle farming. The discovery of just one similar-sized, same-composition object to Hoba, would immediately negate the single body model described here. Given the terrestrial residency time, its mass and

its fall location we can reasonably exclude the possibility of Hoba being a transported mass – that is via glacial transport or by human means. Indeed, the American Museum of Natural History tried to purchase the Hoba meteorite in 1954 but eventually withdrew its offer after all attempts to move it failed – it was this action, in fact, that resulted in the meteorite being declared a national monument in 1955 (http://www.mme.gov.na/gsn/posters/geological-attractions/meteorites.pdf).

One advantage of the shallow entry, slow velocity atmospheric path model is that by the time the meteoroid is close to landing, much of its forward momentum has been lost and the meteorite essentially hits the ground vertically. This is especially so when the large face is orientated forward, as can be seen from column 7 of table 2. Accordingly the uncertain effects associated with oblique angle impacts are less of a concern. Indeed, the size of the initial impact crater associated with the fall of the Hoba meteorite can be readily estimated from the equations used in the Earth Impact Effects Program (EIEP) as developed by Collins, Melosh and Marcus (2005) – specifically, there equations 21 through 26. For an initial mass of 1.15×10^5 kg, σ ($s^2 m^{-2}$) = 1.0×10^{-8}, we obtain a Hoba mass meteorite on the ground and a simple crater having an estimated diameter of about 20 m with a depth of about 5 m. A direct comparison between our calculations and the EIEP is not straightforward since the EIEP does not allow for ablation mass loss and it also adopts a constant angle of atmospheric flight. None the less, similar crater sizes to ours (after impact angle scaling) are obtained with the EIEP program – as one would expect. Given the location and local climate of the fall site, a crater with the derived dimensions of 20 meters might reasonably be lost through erosion over the 80,000 year terrestrial residency time derived for the Hoba meteorite. While the Hoba site has been greatly disturbed since the meteorite was first discovered (especially during the construction of its present monument setting), we note that the ground directly beneath the meteorite may yet hold some small amount of detail relating to the original crater breccia lens.

The observation that even under ideal circumstances the production a Hoba mass meteorite, with an impact velocity of a few hundred meters per second, upon the ground,

is only just obtainable plays directly into the expectation that such large finds must be rare. If we assume a progenitor mass of order 5×10^5 kg for the Hoba meteorite, then the global flux of such objects is about 10^{-3} per year (Brown et al, 2002). Given that 70 percent of Earth's surface is covered by oceans, and that ataxites make-up of order 2 percent of known iron meteorite samples (which in turn constitute about 5 percent of all meteorite falls - Buchwald, 1975) the most likely time interval between the arrival of land impacting, non-fragmenting, Hoba mass ataxite meteorites will be of order 5×10^6 years.

While Hoba is the most massive of all known meteorites, it is not necessarily the most massive meteorite that could possibly exist on Earth's surface. In an earlier study, for example, Artemieva and Bland (2003) have suggested that low velocity (V_∞ = 11 km/s), low entry angle ($\theta \approx 10^o$ at 100 km altitude – see equation A7), asteroid impacts might conceivably produce small-crater forming ($V_{imp} < 2$ km/s) iron meteorites with masses up to 26,000 tonnes on Earth's surface. The multiplicative factor of four over the Hoba mass comes about simply because Artemieva and Bland allow for fragmentation of the incoming asteroid to take place. Indeed, the pre-entry mass of the iron meteoroid considered by Artemieva and Bland (2003) was 10^{10} kg, and a shower of some 35 fragments was produced for a total meteorite ground mass of some one-million tons. Artemieva and Bland further argue that the arrival rate of low impact velocity, meteorites with masses greater than 10,000 tonnes is of order 10^7 years.

We have argued above that it is the form of the atmospheric flight path, as well as the shape and orientation of the meteorite, that is of vital importance with respect to producing the Hoba mass meteorite – that is to slow its velocity below the few hundred meters per second threshold for impact survival. Additionally, it is apparently no accident that Hoba is an ataxite meteorite, as opposed to some other iron meteorite class (octahedrite or hexahedrite). By being an ataxite, and thereby having a relatively uniform internal structure with relatively high yield strength (Furnish et al, 1995), Hoba was able to survive at an impact speed of order 200 m/s. Other iron meteorite types, with characteristically lower yield strengths, would require an impact speed of perhaps 100 m/s in order to survive ground contact. While such small speeds can be realized (see

figure 3) within the scenario being studied, the implication is that, for a given progenitor mass, with all other parameters being the same, only smaller mass meteorites will be realized.

We have not specifically investigated in this study the very small range of impact angles, situated close to the atmospheric skip-limit, for which the direct capture of a meteoroid into temporary Earth orbit can take place. Under this scenario the meteoroid might in principle travel many thousands of kilometers before finally returning to space or impacting the Earth's surface. The latter situation appears to have occurred, for example, with the *Great Meteor* of 18 August 1783, seen along the length of Great Britain and into France (Beech, 1989), and in the Chant fireball procession of 9 February 1913 (Chant, 1913; Mebane, 1956). The Chant fireball group of meteoroids in particular entered Earth's atmosphere above the Canadian prairies, traveled past the Cities of Toronto and New York and were seen as far south and east as the island of Bermuda – the estimated ground path covered by this remarkable procession is of order 10,000 km. For such temporary capture to take place a meteoroid must lose some angular momentum via ablation and deceleration, but not too much that it ends up rapidly impacting the Earth's surface. Hills and Goda (1997) have specifically estimated the probability that an iron meteoroid, undergoing a grazing atmosphere interaction, ends up in temporary orbit about the Earth and find that of order one in one-thousand will do so for initial velocities in the range 11.2 to 20 km/s. Such precise capture events are clearly going to happen only very rarely, but it may be the case that such complications need to be investigated still further in order to explain the Hoba meteoroid (this work is presently in progress).

References

Ahrens, T. J., Anderson, W. W., and Zhao, Y. 1995. Air Force Office of Scientific Research final report: TR-95-0493.

Artemieva, N. A., and Bland, P. A. 2003. 66th Ann. Met. Soc. Meeting, paper 5153.

Baldwin, B., and Sheaffer, Y. 1971. J. Geophys. Res. **76**, 4653.

Bauer, C. A. 1963. J. Geophys. Res. **68**, 6043.

Beech, M. 1989. JBAA. **99**, 130.

Beech, M. 2001. MNRAS. **326**, 937.

Beech, M. 2011. WGN, the journal of IMO, **39**, 9.

Bland, P. A., Cintala, M. J., Horz, F., and Cressey, G. 2001. LPS XXXII, paper 1764.

Borovicka, J., and Spurny, P. 2008. Astron. Astrophys. **485**, L1.

Bottke, W. F. Nolan, M. C., Greenberg, R, and Kolvoord, R. A. 1994. *In Hazards due to comets and asteroids*. Gehrels, T., Matthews, M. S., and Schumann, A (Eds.). University of Arizona Press. p. 337.

Bottke, W. F., Love, S., Tystell, D., and Glotch, T. 2000. Icarus, **145**, 108.

Bronshten, V. A. 1983. *Physics of Meteoric Phenomena*. D. Reidel Pub. Dordrecht.

Brown, P., Spalding, R. E., ReVelle, D. O., Tagliaferri, E., and Worden, S. P. 2002. Nature, **420**, 294.

Brown, P., and 6 co-authors. 2008. Asteroids, Comets, Meteors (2008), Baltimore, Maryland, paper 8097.

Buchwald, V. F. 1975. *Handbook of iron meteorites, their history, distribution, composition and structure*. University of California Press.

Ceplecha, Z. 1994. A&A. **283**, 287.

Ceplecha, Z., and ReVelle, D. O. 2005. MAPS. **40**, 35.

Chant, C. A. 1913. JRASC. **7**, 145.

Collins, G. S., Elbeshausen., Davison, T. M., Robbibs, S. J., and Hynek, B. M. 2011. Earth Plan. Sci. Lett. **310**, 1.

Collins, G. S., Melosh, H. J., and Marcus, R. A. 2005. MAPS. **40**, 817.

Cook, D. L., Wadhwa, M., Davis, A. M., and Clayton, R. N. 2006. LPS XXXVII, paper 2116.

Cox, A. N (Ed.). 1999. *Allen's Astrophysical Quantities*. Springer, New York.

Davison, T. M., Collins, G. S., Elbeshausen, D., Wünnemann, K. and Kearsley, A. 2011. MAPS. **46**, 1510.

Fernie, J. D. 1967. JRASC. **61**, 127.

Furnish, M. D., Boslough, M. B., Gray III, G. T., and Remo, J. L. 1995. Int. J. Impact Eng. **17**, 341.

Golden, D. C., Ming, D. W., and Zolensky, M. E. 1995. Meteoritics, **30**, 418.

Hills, J. G., and Goda, M. P. 1997. Planet. Space Sci. **45**, 595.

Hirata, T., and Masuda, A. 1992. Meteoritics, **27**, 568.

Johnson, A. A., Remo, J. T., and Davis, R. B. 1979. J. Geophys. Res. **84**, 1683.

Jones, W. G., Smith, P. F., Homer, G. J., Lewin, J. D. and Walford, H. E. 1989. Zei. Phys. C. **43**, 349.

Lowry, S. C. and 10 co-authors. 2007. Sci. **326**, 272.

Luyten, W. J. 1930. Pop. Astron. **38**, 13.

Matsumoto, M., Ishizaki, H., Matsuoka, C., Daito, Y., Ichikawa, Y., and Shimahara, A. 1998. J. Wind Eng. Indust. Aerodyn. **77**&**78**, 531.

McCorkell, R. H., Fireman, E. L., D'Amico, J., and Thompson, S. O. 1968. Meteoritics, **4**, 113.

Mebane, A. D. 1956. Meteoritics, **1**, 405.

Melosh, H. J. 1989. *Impact cratering: A geological process*. OUP. Oxford.

Melosh, H. J., and Goldin, T. J. 2008. LPS XXXIX, paper 2457.

Okeefe, J. D., and Ahrens, T. J. 1982. J. Geophys. Res. **87**, 6668.

Passey, R. R., and Melosh, H. J. 1980. Icarus, **42**, 211.

Petrovic, J. J. 2001. J. Material Sci. **36**, 1579.

Pierazzo, E. and Artemieva, N. A. 2005. LPS XXXVI, paper 2325.

Pierazzo, E., and Melosh, H. J. 2000. ARE&PS. **28**, 141.

Popova, O., + 6 co-authors. 2011. MAPS. **46**, 1525.

Rawcliffe, R. D., Bartky, C. D., Li, F., Gordon, E., and Carta, D. 1974. Nat. **247**,449.

ReVelle, D. O., and Ceplecha, Z. 1994. A&A. **292**, 330.

ReVelle, D. O., and Ranjan, R. S. 1988. BAAS. **20**, 862.

Shoemaker, E. 1962. In, *Physics and Astronomy of the Moon.* Kopal, Z (Ed.). Academic Press, New York. p. 283.

Spargo, P. E. 2008. Mon. Not. Astron. Soc. South Africa. **67**, 85.

Spencer, L. J. 1932. Mineral. Mag. **23**, 1.

Svetsov, V. V., Nemchino, I. V., and Teterev, A. V. 1995, Icarus, **116**, 131.

Tancedi, G., and 16 co-authors. 2008. Asteroids, Comets, Meteors Conference (2008), Baltimore, Maryland, paper 8260.

Young, D. F., Munson, B. R., Okiishi, T. H., and Huebsch, W. W. 2010. *A Brief Introduction to Fluid Mechanics*. J. Wiley and Sons, New Jersey.

Appendix: The equations of motion and ablation

Under the non-plane parallel atmosphere approximation (see figure A1) the equations of meteoroid ablation and motion are as follows:

$$\frac{dV}{dt} = -\Gamma \rho_{atm}\left(\frac{A}{m}\right)V^2 + g\sin(\theta) \qquad \text{A1}$$

$$\frac{dm}{dt} = -\left(\frac{\Lambda}{2\zeta}\right)\rho_{atm} A V^3\left(\frac{V^2 - V_{dark}^2}{V^2}\right) \qquad \text{A2}$$

$$\frac{d\theta}{dt} = \left(\frac{1}{mV}\right)\left(mg\cos(\theta) - \tfrac{1}{2}C_{lift}\rho_{atm}AV^2\right) - \frac{V\cos(\theta)}{R+h} \qquad \text{A3}$$

$$\frac{dh}{dt} = -V\sin(\theta) \qquad \text{A4}$$

$$\frac{dX}{dt} = \frac{V\cos(\theta)}{1+h/R} \qquad \text{A5}$$

where m is the mass, V is the velocity, A is the surface area presented to the oncoming airflow, g is the acceleration due to gravity at height h, R = 6371 km is the radius of the Earth, ρ_{atm} is the atmospheric density at altitude h, θ is the flight angle to the horizon, and C_{lift} is the lift coefficient. The term V_{dark} in equation A2 is the dark-flight velocity limit, such that for $V < V_{dark}$ = 2 kms^{-1} vigorous mass loss due to ablation is assumed to have stopped. Equation A5 describes the down-range ground track along the Earth's surface.

The atmospheric density profile is taken to be a fourth-order polynomial fit to height and is based upon the US Standard Atmosphere model described in table 11.21 of *Allen's Astrophysical Quantities* (Cox, 1999). Accordingly we have for $1 \le h(\text{km}) \le 1000$, the expression:

$$\log \rho = \sum_{0}^{4} a_i (\log h)^i \qquad \text{A6}$$

where the density is expressed in units of kg/m^3, and the height is expressed in kilometers. The constants a_i are: 0.0821, -2.274, 6.4318, -5.4622, 1.0152 for i = 0, 1, 2, 3, 4 respectively.

While the simulation assumes that the area A presented by the meteoroid to the oncoming airflow is constant, the depth dimension of the meteoroid will decrease as the leading edge is ablated. The depth dimension D is tracked according to the instantaneous meteoroid mass, with $D = m / \rho_{met} A$.

There is no specific definition or accepted convention for specifying the initial beginning height in simulations such as the ones being presented here. Often, a beginning altitude of 100 km is adopted since it is only below this height range that atmospheric heating, fragmentation and deceleration effects become important. This study adopts a 500 km altitude starting height, however, to allow for the possibility of pre-ablation trajectory alteration as a consequence of the gravitational interaction between the Earth and the in-coming meteoroid. If the gravitational interaction is ignored, then the straightforward geometrical relationship between our impact angle θ, specified at h = 500 km, and the impact angle θ_{100} specified at an altitude of h = 100 km, is

$$\cos(\theta_{100}) = \left(\frac{R_{Earth} + 500}{R_{Earth} + 100} \right) \cos(\theta) \qquad \text{A7}$$

Accordingly, for example, an impact angle of θ_{100} = 10^o at h = 100 km corresponds to θ = 22^o at h = 500 km.

Figures and figure Captions

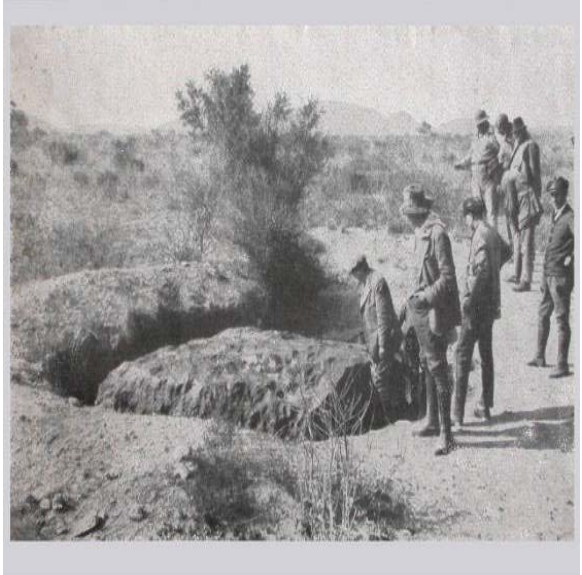

Figure 1. Inspection of the Hoba meteorite on 5 September 1929 by an excursion of attendees to the International Geological Congress held in Pretoria, South Africa (Spencer, 1932). This picture gives some idea of the meteorite's scale and it illustrates the terrain in which the meteorite was initially found. The Hoba meteorite was declared a Namibian National Monument in 1955, and now sits at the center of an amphitheater-like structure.

Figure 2. Etched slab-section from the Hoba meteorite showing its uniform (Widmanstätten pattern free, ataxite) interior structure. The parallel dark bands were likely produced through low-velocity shock and heating alteration (Buchwald, 1975). The lower straight edge of the slab is a little under 16 cm long. Image courtesy of the Smithsonian Institution and Linda Welzenbach.

Figure 3. Initial mass versus impact velocity when the initial velocity is fixed at 11.2 km/s, the large face is orientated to the oncoming airflow and the entry angle is at its minimal value for ground impact: $\theta = 16^{o}$. The various curves are parameterized according to the ablation coefficient σ (s^2/m^2) adopted in the calculation. The vertical line separates out the domain in which, to the right, the ground impact mass is larger than 60,000 kg (the Hoba ground mass), and to the left where the ground impacting mass is smaller than 60,000 kg. The horizontal dotted line indicates the boundary above which Hoba mass meteorites might possibly be produced.

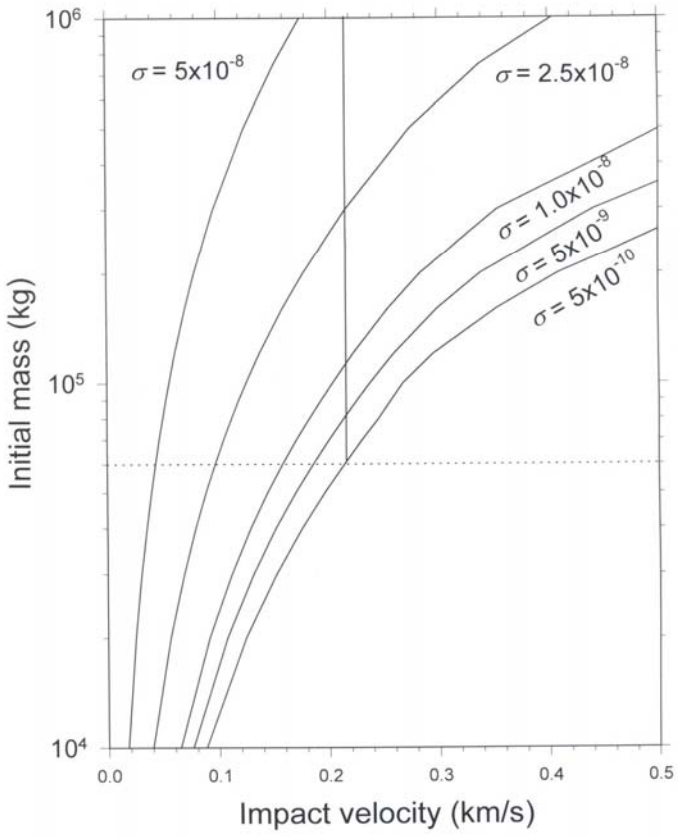

Figure A1. Schematic diagram of the encounter geometry model. *R* corresponds to Earth's radius, θ is the initial impact angle and *Z* is the zenithal angle.

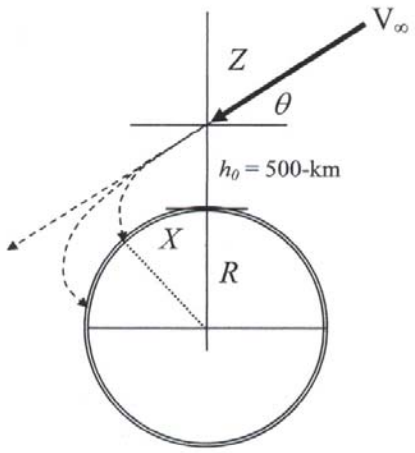

Table and table caption

Initial values	**Quantity adopted**
Meteoroid density	7800 kg/m^3
Meteoroid Yield strength	700 MPa (upper limit value)
Energy of vaporization	5 x 10^6 J/kg
Heat transfer coefficient	0.005 – 0.5
Drag coefficient	1.2 (see text for details)
Lift coefficient	0.0 (assumed value)
Ablation coefficient	$5.0x10^{-10}$ – $5.0x10^{-8}$ s^2/m^2
Starting altitude	500 km
Initial velocity	11.2 km/s
Impact angle	0^o (horizontal) - 90^o (vertical)
Final values	
Impact velocity	Smaller than a few 10^2 m/s
Final mass	60,000 kg
Final dimensions	2.95 x 2.84 x 0.9 m

Table 1. Summary of adopted parameters and final impact characteristics. See text for discussion and details.

Face	σ (s^2m^2)	θ_0 (deg.)	V_∞ (km/s)	Range ($x10^3$ km)	V_{imp} (km/s)	θ_{imp} (deg.)	M_{imp} ($x10^4$ kg)	$P_{ram, max}$ (MPa)
L	$2.5x10^{-8}$	45	11.2	0.497	0.13	87.9	1.98	21.5
L	$2.5x10^{-8}$	45	15.0	0.500	0.07	90.0	0.58	28.4
S	$2.5x10^{-8}$	45	11.2	0.502	1.70	42.9	1.96	61.9
S	$2.5x10^{-8}$	45	15.0	0.508	0.12	82.0	0.57	87.9
L	$5.0x10^{-9}$	45	11.2	0.502	0.87	44.2	7.23	30.4
S	$5.0x10^{-9}$	45	11.2	0.502	5.68	42.7	7.75	77.7
L	$1.0x10^{-8}$	75	11.2	0.131	1.12	74.6	5.23	38.0
L	$1.0x10^{-8}$	45	11.2	0.502	0.41	48.2	5.23	27.7
L	$1.0x10^{-8}$	25	11.2	1.169	0.20	71.4	5.22	14.0
L	$1.0x10^{-8}$	16	11.2	2.927	0.20	81.4	5.22	2.2
L	$1.0x10^{-8}$	25	15.0	1.241	0.16	86.1	3.18	18.5
S	$1.0x10^{-8}$	75	11.2	0.132	6.65	74.4	6.38	93.8
S	$1.0x10^{-8}$	45	11.2	0.502	4.92	42.6	5.77	71.5
S	$1.0x10^{-8}$	25	11.2	1.181	1.56	20.8	5.21	42.5
S	$1.0x10^{-8}$	25	15.0	1.262	0.50	26.3	3.17	58.5
S	$1.0x10^{-8}$	16	11.2	2.066	0.37	46.9	5.21	6.2

Table 2. Summary of simulation results for various entry conditions and physical parameters. The face area is defined as being large (L) when the 2.95 x 2.84 profile faces the oncoming airflow and small (S) when the 2.84 x 0.9 profile faces the oncoming airflow. The symbols V_{imp}, θ_{imp} and M_{imp} correspond to the impact velocity, impact angle to the horizon, and the impacting mass; $P_{ram, max}$ corresponds to the maximum ram pressure, in mega-Pascals, realized during atmospheric flight.